0254-6124/2023/43(4)-0724-12 *Chin. J. Space Sci.* 空间科学学报

FENG Shuai, WANG Ronglan. Meteoroid and Space Debris Risk Assessment for Satellites Orbiting the Earth/Moon. *Chinese Journal of Space Science*, 2023, **43**(4): 724–735. DOI:10.11728/cjss2023.04.2022–0065

Meteoroid and Space Debris Risk Assessment for Satellites Orbiting the Earth/Moon*

FENG Shuai WANG Ronglan

(*National Space Science Center*, *Chinese Academy of Sciences*, *Beijing* 100190)

(*University of Chinese Academy of Sciences*, *Beijing* 100049)

(*State Key Laboratory of Space Weather*, *National Space Science Center*, *Chinese Academy of Sciences*, *Beijing* 100190)

(*Key Laboratory of Science and Technology on Environmental Space Situation Awareness*, *Chinese Academy of Sciences*, *Beijing* 100190)

Abstract Interplanetary meteoroids and space debris can impact satellites orbiting the Earth or spacecraft traveling to the Moon. Targeting China Space Station (CSS), 7 satellites selected from the constellation of Beidou Navigation Satellite System Phase III (BDS-3), and 3 spacecraft orbiting the Moon, we have adopted in the paper the Meteoroid Engineering Model 3, Divine-Staubach meteoroid environment model, and Jenniskens-McBride meteoroid steam model to analyze the meteoroid environment with the mass range of 10^{-6}～10 g. Orbital Debris Engineering Model 3.1 space debris model is used to analyze the orbital debris environment faced by these satellites. The flux of space debris with a size larger than 100 μm is compared with that of the meteoroids. The results show that the space debris flux encountered by China Space Station is much higher than that of the meteoroids with sizes in the above range. And quite the opposite, the meteoroids flux impacting the 7 satellites from the BDS-3 is higher. Upon adopting the double-layer Whipple protection measure, the catastrophic collision flux of these satellites encountering meteoroids is about 10^{-6} times of that without protection, or even less, implying that the Whipple protection effectively guarantees the safety of the satellites in orbit. Besides, it is also found that the flux of the high-density meteoroid population encountered by each satellite is greater than that of the low-density population, whereas the impact velocity is lower for each satellite. These results can aid the orbit selection and the protection design for satellites and spacecraft.

Key words Meteoroid environment model, Space debris model, Ballistic limit equation, Impact risk assessment

Classified index P223

0 Introduction

In the Earth's orbit space, the spacecraft is impacted by both meteoroids and space debris, while in the Moon's orbit space, it is mainly impacted by the meteoroids. The flux of meteoroids is relatively stable over time, and the amount of space debris increases with the increasing human space activities, especially the deployment of large constellations in recent years[1]. European Space Agency (ESA) estimates that the number of flying objects in

* Supported by the National Natural Science Foundation of China (42074224), Key Research Program of the Chinese Academy of Sciences (ZDRE-KT-2021-3) and Pandeng Program of National Space Science Center, Chinese Academy of Sciences

Received November 3, 2022. Revised June 25, 2023

E-mail: fengshuai20@mails.ucas.ac.cn

©The Author(s) 2023. This is an open access article under the CC-BY 4.0 License (https://creativecommons.org/licenses/by/4.0/)

outer space can be about 130 million in 2019[2], and with the current space debris status and scheduled space missions, fragmentations increase the cross-section of satellites on orbit[3], and the collision probability will rapidly rise every 7 years[4]. Thus, to ensure the sustainable development of the space environment, meteoroid and space debris mitigation measures are needed to take, and the impact risk of meteoroids and space debris also needs to be assessed[5].

Currently, the meteoroid and space debris models or software tools that are widely used include Meteoroid Engineering Model (MEM), Bumper, Orbital Debris Engineering Model (ORDEM), Meteoroid and Space Debris Terrestrial Environment Reference (MASTER), and Debris Risk Assessment and Mitigation Analysis (DRAMA). Cooke *et al.*[6] used MEMR2 and ORDEM 3.0 models to analyze the flux of meteoroids and space debris penetrating 1 mm thick aluminum plates in 6 directions of spacecraft in the Earth orbit space. They found that the penetrating flux of meteoroids on the surface facing the zenith is greater than that of space debris while, the penetrating flux of space debris on the surface facing the ram, port and starboard is higher than that of meteoroids between 250 km and 2500 km. Moorhead *et al.*[7] used the later models, *i.e.* MEM 3 and ORDEM 3.1, addressing a similar problem and found that the penetration rate of meteoroids varies by an order of 2 in magnitude whereas the space debris penetration rate changes by an order of 7 in magnitude between the orbits from 100 km to 100 000 km.

Krag *et al.*[8] investigated the impact of micro-meteoroid and orbital debris onto a solar array in 2017. Hoffman *et al.*[9] used the Bumper-3 code to assess the failure of Extravehicular Mobility Unit (EMU) for Extravehicular Activity (EVA) on International Space Station (ISS) caused by meteoroids and space debris[10]. Further, they employed MEM 3 and ORDEM 3.1 to assess the damage risk of EMU, and found that for a period of 6.5 h EVA, the impact damage risk is rather small. Evans *et al.*[11] provides an overview of the modeling theory and functionality of the Manned Spacecraft Crew Survivability software code, which is used to predict the probability of several outcomes of micrometeoroid and orbital debris penetration for ISS. Actually, according to the measured value, the damage found in post-flight inspection of the Pressurized Mating Adapter cover and the returned airlock shield panels of ISS is consistent with the predicted results of the Bumper 3 risk assessment code using the ORDEM 3.0 and MEMR2 models[12]. Additionally, Lorenzo Olivieri *et al.*[13] performed the space debris assessment for the large constellations in Low-Earth Orbit, and found that reducing the lifetime of individual satellites in a constellation would cause an overall increase in the total number of uncontrolled resident objects.

Currently, few researchers have systematically assessed meteoroid risk for satellite constellations. Therefore, operational satellites and spacecraft including the China Space Station (CSS) in Low Earth Orbit (LEO), 7 satellites in the satellite constellation of Beidou Navigation Satellite System Phase III (BDS-3), and 3 satellites orbiting the Moon orbit are tested against a variety of meteoroid and space debris models in this paper. MEM 3, Divine-Staubach meteoroid environment models, and Jenniskens-McBride meteoroid stream model are used to compute the meteoroid flux encountered by each satellite. The double-layer Whipple protective structures are considered. ORDEM 3.1 model is used to generate the space debris environment for the 8 satellites orbiting the Earth. Both the fluxes of meteoroids and space debris and the impact risk assessments are compared and analyzed, which can provide support for spacecraft structure and orbit design as well as on-orbit maintenance. One application is the installation of the ISS protective shields based on the calculated risk assessment data to help enhance spacecraft protection in the maximum risk zones[14].

1 Meteoroid Environment Model and Impact Risk Analysis Method

In this section, we briefly discuss the meteoroid environment models that we have adopted to analyze the environments faced by the 8 satellites in the Earth's orbit space and the 3 satellites in the Moon's orbit space. All the satellites are developed in China, and the 8 satellites orbiting the Earth are currently in operation.

1.1 Meteoroid Environment Model

Meteoroids are granular particles in the interplanetary space orbiting the Sun, generally including sporadic me-

teoroids, meteoroid streams, *etc*. A complete meteoroid environment model includes: (1) mass-density distribution, (2) velocity distribution, and (3) flux-mass/diameter distribution. The meteoroid flux F is defined as the number of particles with mass greater than m passing through any configuration surface per square meter per year generally ($m^{-2}\cdot a^{-1}$), which refers to the average accumulation number of sporadic meteoroids and meteoroid steam. In this paper, MEM 3 and Divine-Staubach meteoroid environment models are selected. MEM 3 can be used to analyze the flux and impact velocity variations of meteoroids in all directions of the spacecraft and the Divine-Staubach model can be used to calculate the catastrophic collision flux and penetrating flux of meteoroids. The results are compared to those obtained from the Jenniskens-McBride meteoroid stream model.

The MEM developed by NASA is based on meteor radar observations, lunar impact craters and zodiacal light observations. It's a parametric model of the spatial distribution of sporadic meteoroids in the solar system from 0.2 to 2.0 AU. NASA released MEM 3.0 in 2019[15], which models meteoroids with mass ranging from 10^{-6} to 10 g. MEM 3 divides the meteoroid environment into two populations: the high-density population consisting of helion and anti-helion meteoroids with a density of about 3.8 $g\cdot cm^{-3}$, and the low-density population with a density of about 0.85 $g\cdot cm^{-3}$, with the latter composed of toroidal and apex meteoroids [16]. According to the output results of MEM 3, this paper mainly discusses 9 directions: ram, wake, port, starboard, zenith, nadir, Earth/Moon, Sun, and anti-Sun.

ESA's MASTER assesses the influence of these particles on space missions by simulating known debris and meteoroids in the Earth space[17]. ESA released MASTER v8.0.3 in April 2022, which improves the automation significantly[18], and embeds both the Divine-Staubach meteoroid environment model (denoted by D-S) and Jenniskens-McBride meteoroid stream model (denoted by J-M) [19]. Jenniskens and McBride established the J-M meteoroid stream model based on naked-eye and photographic observations of amateur astronomers around the world from 1981 to 1991[20]. In the D-S model, the average density of meteoroids originating in asteroids is about 3.5 $g\cdot cm^{-3}$, and the density ρ of meteoroids originating in other parent bodies is given by

$$\rho=\begin{cases}2.0, & m<10^{-6};\\ 1.0, & 10^{-6}\leqslant m\leqslant 10^{-2};\\ 0.5, & m>10^{-2}.\end{cases} \tag{1}$$

Here unit of ρ is $g\cdot cm^{-3}$, and m is the mass of the meteoroid (unit g).

NASA's ORDEM can be used to describe the space debris environment faced by spacecraft and can give the flux data of space debris at 6 different sizes. NASA released ORDEM 3.1 in December 2019 which uses the latest and highest-fidelity datasets derived from radar and optical detections and in situ detections[21]. The model uses state-of-the-art analytical techniques to update the model population[22]. ORDEM 3.1 categorizes space debris into 5 types: intacts, low-density fragments, medium-density fragments and microdebris, high-density fragments and micro debris, and sodium-potassium eutectic coolant droplets for Radar Ocean Reconnaissance Satellite reactors. The densities are about 2.8, 1.4, 2.8, 7.9 and 0.9 $g\cdot cm^{-3}$, respectively.

In fact, meteoroids with a mass smaller than 10^{-6} g have a very small possibility of causing damage to spacecraft in orbit. According to the limiting conditions of the mass of the meteoroid in each model, the meteoroid environment with mass ranging from 10^{-6} to 10 g will be discussed in the risk assessment of the spacecraft. And based on the output results of each model, the particle velocities discussed in this paper are relative to the spacecraft unless otherwise specified.

1.2 Ballistic Limit Equation

The expected damage on a satellite surface as the result of a meteoroid or space debris impact can be assessed through empirically derived design equations by providing crater depths or diameters as a function of the particle properties[23]. The Ballistic Limit Equation (BLE) defines the failure limit of the spacecraft structure on the basis of the properties of the particles, and is used to calculate the critical particle diameter (that is, particles with the velocity v, the impact angle α, and the diameter greater than d_c colliding with the protective layer will penetrate) [24]. BLE can be divided into single-layer BLE and multi-layer BLE. In this paper, the satellite protection type is set as double-layer Whipple plate protection, and its BLE uses the Christiansen equation [25]:

$$d_{\mathrm{c}}=\begin{cases}\left(\dfrac{t_{\mathrm{b}}\sqrt{\dfrac{\sigma}{40}}+t_{\mathrm{s}}}{0.6\sqrt{\rho_{\mathrm{p}}}v^{\frac{2}{3}}(\cos\alpha)^{\frac{5}{3}}}\right)^{\frac{18}{19}}, & v_{\mathrm{n}}\leqslant 3;\\ \dfrac{1.071t_{\mathrm{b}}^{\frac{2}{3}}S^{\frac{1}{3}}\left(\dfrac{\sigma}{70}\right)^{\frac{1}{3}}\left(\dfrac{v\cos\alpha}{4}-0.75\right)}{\rho_{\mathrm{p}}^{\frac{1}{3}}\rho_{\mathrm{s}}^{\frac{1}{9}}}+\\ \left(\dfrac{t_{\mathrm{b}}\sqrt{\dfrac{\sigma}{40}}+t_{\mathrm{s}}}{1.248\sqrt{\rho_{\mathrm{p}}}\cos\alpha}\right)^{\frac{18}{19}}\left(1.75-\dfrac{v\cos\alpha}{4}\right), & 3<v_{\mathrm{n}}<7;\\ \dfrac{3.918\,t_{\mathrm{b}}^{\frac{2}{3}}S^{\frac{1}{3}}\left(\dfrac{\sigma}{70}\right)^{\frac{1}{3}}}{\rho_{\mathrm{p}}^{\frac{1}{3}}\rho_{\mathrm{s}}^{\frac{1}{9}}(v\cos\alpha)^{\frac{2}{3}}}, & v_{\mathrm{n}}\geqslant 7.\end{cases}\tag{2}$$

Where d_{c} is the critical particle diameter in cm; the subscripts p, s, and b denote the parameters of the particle, the first protective layer, and the second rear wall (bulkhead), respectively; t is the thickness of the plate in cm; ρ is the density in g·cm^{-3}; σ is the yield strength of the rear wall in MPa; α is impact angle, in degree; v is the impact velocity in km·s^{-1} and v_{n}=$v$cosα; S is the distance between the first protective layer and bulkhead, in cm.

Some of the above models use size as one of the parameters, while others use mass. In order to facilitate the comparative analysis, this paper assumes that the shape of the meteoroid is spherical, so the mathematical expression of the relationship between the mass and diameter of the meteoroid is as follows [26]:

$$m=\frac{\rho\pi d^3}{6}.\tag{3}$$

Therefore, the critical particle mass m_{c} can be calculated according to Eq.(2) and (3). Similar to d_{c}, m_{c} means that a particle with mass greater than or equal to m_{c} will penetrate when impacting the protective layer with the velocity v and the impact angle α.

1.3 Impact Risk Analysis Method

Particles with high velocities, when colliding with spacecraft produce large impact energy. For instance, the energy of a particle with a mass of 1 g, whose speed is 10 km·s^{-1}, is equal to the load energy of a mass of 1 ton, falling from a height of 5 m for CSS [27]. When assessing the risk of spacecraft caused by meteoroids or space debris, the Energy-to-Mass Ratio (EMR, the symbol E is employed as a representation for the acronym EMR here) can be used to measure whether or not an impact is a catastrophic collision event. If the value of EMR is greater than 40 000 J·kg^{-1}, it is considered that the impact event is a catastrophic collision. The mathematical expression of EMR is given by[28]:

$$E=\frac{m_{\mathrm{p}}v^2}{2m_{\mathrm{s}}}.\tag{4}$$

Here m_{p} is the mass of the particle; v is the velocity of the particle impacting the spacecraft; m_{s} is the mass of the spacecraft; the unit of EMR is J·kg^{-1}.

It is assumed that the probability of the spacecraft experiencing particle impact follows Poisson distribution [29], *i.e.* the probability P of the spacecraft encountering n times of collision is given by

$$P=\frac{N^n}{n!}e^{-N}.\tag{5}$$

and

$$N=FAT.\tag{6}$$

Here N is the average number of collisions between spacecraft and particles; F is the flux of spacecraft encountering particle impacts; A is the impact cross-sectional area of the spacecraft; T is the operating time of the spacecraft. For the convenience of comparison, this paper assumes that the impact cross-sectional area A of the spacecraft with the meteoroids or space debris is 1 m^2, and the time T of the spacecraft is 1 year.

Thus, the probability that a spacecraft does not collide with any particles (n=0), in other words, the probability of non-impact is

$$P_N=e^{-N}.\tag{7}$$

Hence, the probability that a spacecraft collides at least once is

$$P_I=1-P_N=1-e^{-N}.\tag{8}$$

2 Meteoroid Risk Assessment for Spacecraft

In this section, we discuss in detail the meteoroid environment faced by the 11 satellites mentioned in the last section.

2.1 Satellite and Its Parameters

It is crucial to analyze the meteoroid environment that CSS may experience because the potentially hazardous granules can not only damage the structure of the station but also threaten the health of the astronauts conducting EVAs. Satellites with three different types of orbits are selected according to the distribution of the BDS-3 satellite constellation. Figure 1 shows the schematic of these satellites: BEIDOU-3 G3 with catalog number 45807 (referred to as G3) in Geostationary Earth Orbit (GEO); 3 satellites BEIDOU-3 IGSO-1, BEIDOU-3 IGSO-2, and BEIDOU-3 IGSO-3 with catalog number 44204, 44337, and 44709 (respectively referred as I1, I2, and I3) in Inclined GeoSynchronous Orbit (IGSO); and 3 satellites BEIDOU-3 M20, BEIDOU-3 M22, and BEIDOU-3 M24 with catalog number 44865, 44794 and 44543 (respectively referred as M20, M22, and M24) in Medium Earth Orbit (MEO). Their characteristic parameters are shown in Table 1.

In the Moon's orbit space, 3 kinds of satellites (MO1, MO2, MO3) in 3 orbits are selected to test against the above models. In the Moon J2000.0 coordinate system, their characteristic parameters and initial state are shown in Table 2, which are based on the orbital parameters of the Chang'E-1 spacecraft, Chang'E-2 spacecraft and Chang'E-5 spacecraft respectively.

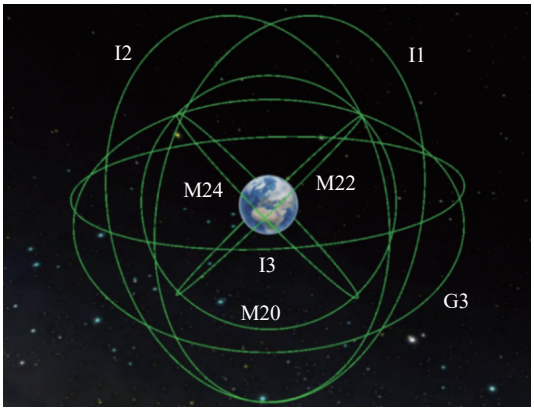

Fig. 1 Schematic of the BDS-3's satellite constellation

It is assumed that the velocity of the particles is perpendicular to the spacecraft surface, *i.e.* the impact angle $\alpha = 0°$. When the satellite adopts double-layer Whipple plate protection, the first protection layer is set as a 0.1 cm thick aluminum plate (Al-6061-T6) and the second layer (bulkhead) is set to 0.2 cm thick aluminum plate (Al-6061-T6), placed 0.5 cm apart [30]. The material properties of Al-6061-T6 are shown in Table 3 [31].

2.2 Meteoroid Flux Calculated by MEM 3 Model

The output file of MEM 3 divides the meteoroid environment of mass ranging from 10^{-6} to 10 g into 2 populations: high-density meteoroid population and low-density meteoroid population. Accordingly, this section discusses the meteoroid flux that the satellites may encounter separately.

For the high-density population, the averaged flux and the averaged colliding velocity of meteoroids for the total 11 satellites in 9 directions are shown in Figure 2

Table 1 Characteristic parameters of the 8 satellites in the Earth orbit space

Satellite	Mass/kg	Average altitude/km
CSS	900 000	393
M20	1060	21528
M22	1060	21528
M24	1060	21528
G3	5400	35786
I1	5400	35786
I2	5400	35786
I3	5400	35786

Table 2 Characteristic parameters and initial Kepler orbital elements of the 3 satellites orbiting the Moon, where *m* is the mass, *h* is the average altitude, *a* is the semi-major axis, *e* is the eccentricity, *i* is the orbital inclination, Ω is the right ascension of ascending node, ω is the argument of perilune, and *M* is the mean anomaly

Satellite	*m* /kg	*h* /km	*a* /km	*e*	*i* /(°)	Ω /(°)	ω/ (°)	*M* /(°)
MO1	2350	194.65	1932.85	0	90	104	0	296
MO2	2480	100	1837.83	0	90	104	0	296
MO3	2480	100	1944	0.01	31	104	74	296

Table 3 Material properties for aluminum Al-6061-T6

ρ /(kg·m^{-3})	Brinell hardness	σ /MPa
2713	95	276

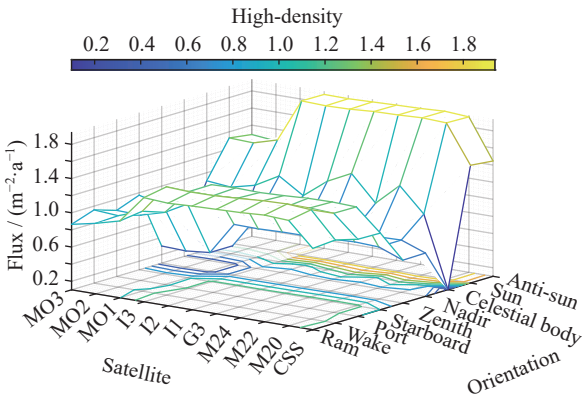

Fig. 2 Averaged impact flux of the high-density meteoroid population in 9 directions for all the 11 satellites

and Figure 3, respectively. Figure 4, together with Figure 5 shows the results of the low-density population for comparison. Especially, the averaged flux and impact velocity of the two meteoroid populations on the surface facing the Earth/Moon are shown in Figure 6. These conclusions can be obtained as followed.

(1) Comparative analysis of the averaged flux for satellites orbiting the Earth/Moon. In the Earth orbit space, the averaged fluxes of CSS encountering the 2 populations are lower than those of other satellites. The average flux of the Earth-facing surface of CSS is about 0.1 m^{-2}·a^{-1}, which is the lowest in the whole field. Compared to the 7 satellites of BDS-3, it is found that the influence of the orbital altitude and inclination on the flux is not obvious. However, the value of the averaged flux fluctuates greatly on the surface facing Earth, which indicates that the Earth's shielding and gravitational focusing may have played a greater role in it on this surface than along other orientations. In addition, the averaged fluxes of high-density and low-density meteoroid populations encountered by MO1, MO2, and MO3 are lower than those encountered by the 8 satellites in the Earth orbit space.

(2) Comparative analysis of the averaged impact velocity for satellites orbiting the Earth/Moon. The average impact velocity of a high-density meteoroid population is lower than that of a low-density population. Without considering the Earth- or Moon-facing surface, for the 10 satellites (CSS not included), it is found that the influence of the orbital altitude and inclination on the average impact velocity is not obvious. For the high-density meteoroid population, CSS has the largest average impact velocity, while the velocity of the 3 satellites in the Moon orbit space is similar to that of the 7 satellites of BDS-3 except for the zenith- or nadir-facing surface. As for the low-density population, the average impact velocity for Moon-orbiting satellites is higher than that for satellites in the Earth orbit space.

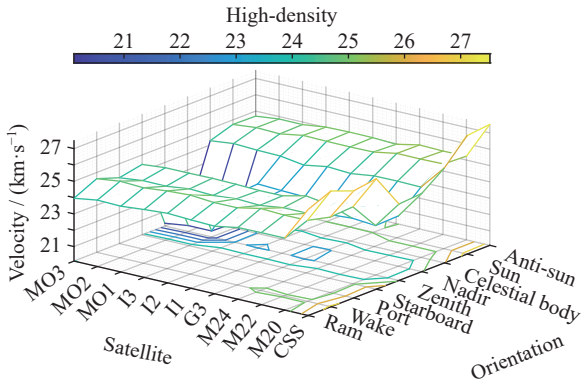

Fig. 3 Averaged impact velocity of the high-density meteoroid population in 9 directions for all the 11 satellites

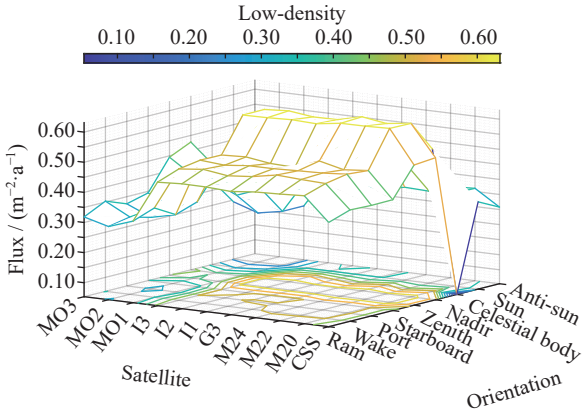

Fig. 4 Averaged impact flux of the low-density meteoroid population in 9 directions for all the 11 satellites

(3) Averaged flux and impact velocity analysis in 9 directions. The average flux of the high-density meteoroid population is higher on the surface facing the Sun or away from the Sun, while the flux on the surface facing the zenith or nadir is lower. Additionally, the impact velocity along the direction facing the zenith or nadir is also lower than that along other directions, especially for

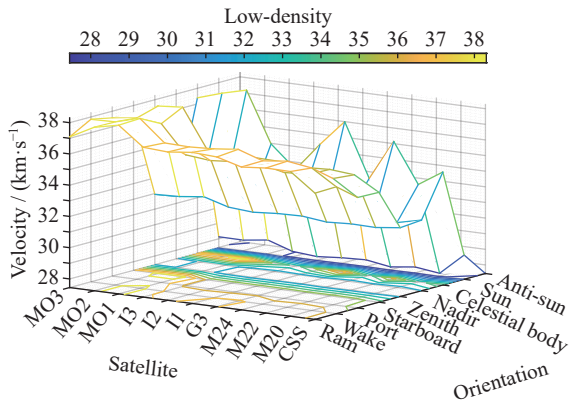

Fig. 5 Averaged impact velocity of the low-density meteoroid population in 9 directions for all the 11 satellites

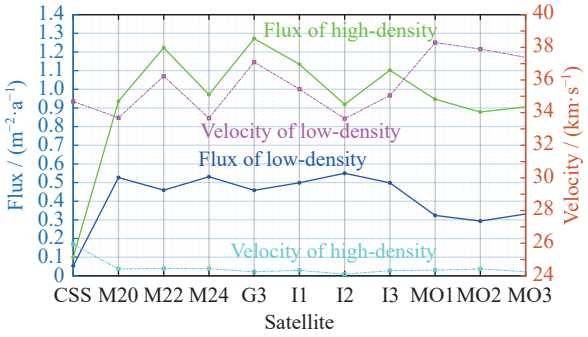

Fig. 6 Averaged flux and velocity on the surface facing Earth/Moon

MO1, MO2, and MO3. For the low-density population, the averaged flux is higher on the surface facing zenith or nadir, and lower on the surface facing the Sun or away from the Sun. The average impact velocity is the lowest on the Sun-facing and anti-Sun-facing surfaces, and higher on the surface facing ram or wake. Additionally, the influence of orbital inclination on the averaged flux and impact velocity of the 2 populations is more obvious in the Earth-facing or the Moon-facing orientation than that in other orientations. The difference of the averaged flux and velocity among the orientations is mainly due to the fact that the orbit of the meteoroid is similar to the orbit of its parent body, which is not isotropic[32].

The averaged total fluxes from all directions encountered by the 11 satellites, together with the ratio of the total fluxes of the high-density and low-density population are shown in Figure 7. These results can be obtained as followed.

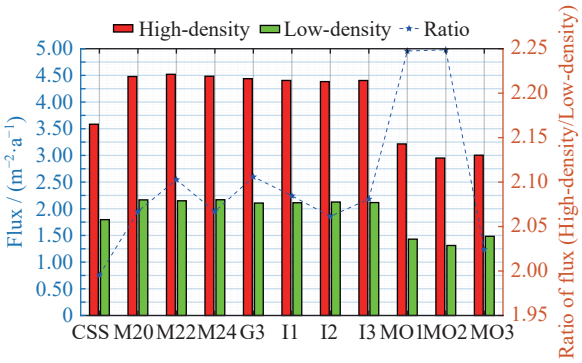

Fig. 7 Averaged total flux for all 11 satellites encountering the high-density and low-density meteoroid populations (the red histogram is the average total flux of the high-density population, and the green histogram is the average total flux of the low-density population). The blue dashed line with the pentagram is the ratio of the total flux of the high-density population over the low-density population

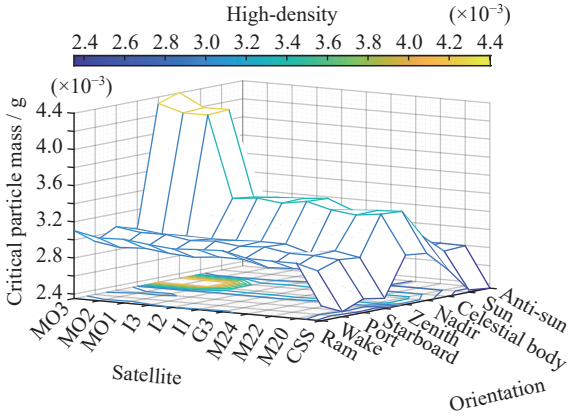

Fig. 8 Critical meteoroid particle mass in 9 directions of 11 satellites encountering the high-density meteoroid populations

(1) The flux of the high-density meteoroid population for each satellite is approximately twice as much as that of the low-density population.

(2) For each satellite orbiting the Moon, the flux is lower than that for every satellite orbiting the Earth.

(3) The total flux of either high-density or low-density meteoroid population for CSS is the lowest in the Earth orbit space.

Figure 8～10 demonstrate the critical mass of the high-density and the low-density meteoroid population for the 11 satellites in 9 orientations, respectively. These conclusions can be acquired as followed.

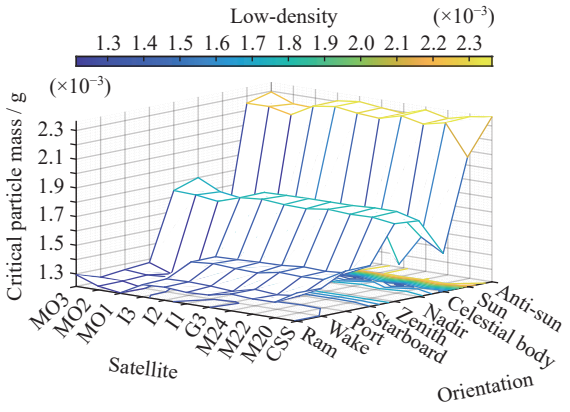

Fig. 9 Critical meteoroid particle mass in 9 directions of 11 satellites encountering the low-density meteoroid populations

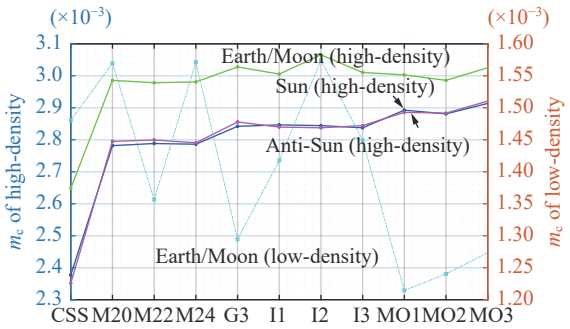

Fig. 10 m_c of the high-density meteoroid population in the directions facing the Earth/Moon, Sun and anti-Sun, and the m_c of the low-density meteoroid population on the surfaces facing the Earth/Moon

(1) The critical mass of the high-density population is the highest in the directions facing zenith and nadir, but lower in the directions facing the Sun and anti-Sun. Moreover, the critical mass for spacecraft in the Moon orbit space is larger than that for satellites in the Earth orbit space, especially on the zenith- and nadir-facing surfaces.

(2) The critical mass of the low-density meteoroid population is the highest on the surfaces facing the Sun and anti-Sun, but lower on the ram- and wake-facing surfaces. Besides, the critical mass in the Moon orbit space is lower than in the Earth orbit space.

(3) In the orientation facing the Earth or the Moon, the orbital inclination plays a more important role in deciding the critical mass of the low-density meteoroid population than the high-density population.

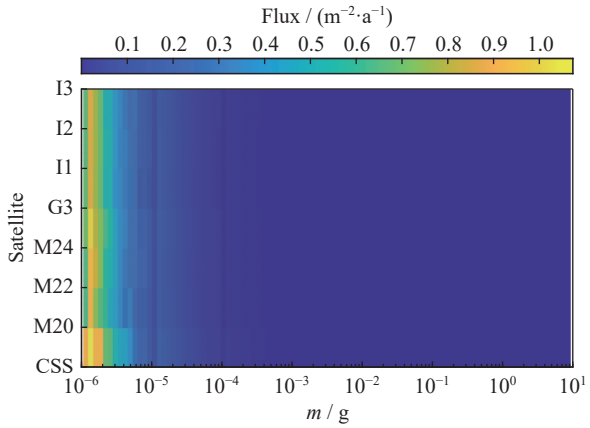

Fig. 11 Dependence of flux on the meteoroid mass for each satellite orbiting the Earth

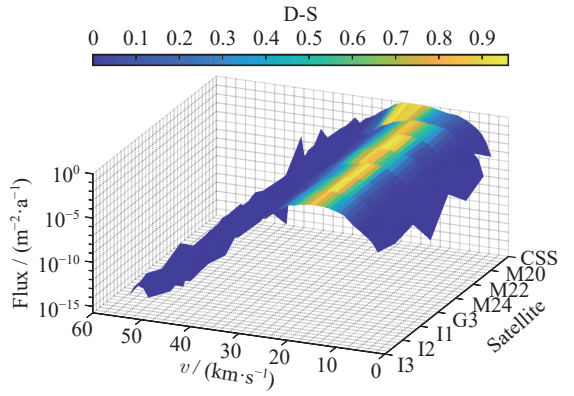

Fig. 12 Dependence of flux on the impact velocity for each satellite orbiting the Earth

2.3 Flux Comparative Analysis of Meteoroids and Meteoroid Streams

For the 8 satellites in the Earth's orbit space, this subsection first uses the D-S model meteoroid environment model to calculate the meteoroid environment, and then the J-M meteoroid stream to calculate the stream flux.

The meteoroid flux as a function of the meteoroid mass for each satellite is shown by the color bar in Figure 11. It can be seen from the figure that the higher mass of the meteoroid, the lower the flux. The dependence of flux on impact velocity is shown in Figure 12, where the velocity of most of the meteoroids encountered by CSS is higher than that of other satellites. Comparing the results among the 7 satellites of BDS-3, it is found that the orbital inclination has a slight influence on the velocity at the peak of the meteoroid flux.

The dependence of the critical diameter on mete-

oroid mass and velocity is shown in Figure 13. Recalling Eq.(1), a similar result for the critical mass is shown in Figure 14. Evidently, both the critical diameter d_c and critical mass m_c decrease with the increase of impact velocity. Particularly, d_c and m_c decrease dramatically with the increase of velocity between 0.5～2.5 km·s^{-1}, where precisely d_c drops from 2.932 to 0.139 mm, and m_c drops from 22.374 to 8.096 g.

The catastrophic collision fluxes F_{EMR1} and F_{EMR2} for the 8 satellites before and after adopting the double-layer Whipple protection measure are calculated by Eq. (4). The results, together with penetrating flux F_{pen} of the satellites taking the protection measure, are shown in Figure 15. We find that the F_{EMR1}, in which case indicated by the subscript 1 all the satellites take no protection, of CSS is about 8.594 m^{-2}·a^{-1} and much higher than that of the BDS-3's satellites. The F_{EMR1} of the 4 satellites in GEO and IGSO is about 0.5 m^{-2}·a^{-1} while the F_{EMR1} of the 3 satellites in MEO is about 0.1 m^{-2}·a^{-1}. After adopting the double-layer Whipple protection measure, the order of the magnitude of F_{pen} is about 10^{-3} and the order of the magnitude of F_{EMR2} is reduced to 10^{-6} for CSS. Although the 3 satellites in MEO have penetrating flux, the catastrophic impact will not likely occur.

For the 8 satellites orbiting the Earth, the fluxes calculated according to the 2 meteoroid stream models are shown in Figure 16. The ratio of $F_{J\text{-}M}$ over $F_{D\text{-}S}$ for CSS is about 1.8×10^{-2}, which is the lowest. The $F_{J\text{-}M}$ for the other 7 satellites is also less than 0.04 times of $F_{D\text{-}S}$. Hence the flux of the meteoroid stream is much lower than that of the meteoroid. However, the meteoroid risk is sufficiently close to the allowable maximum during periods with some maximum meteor shower activities, which needs to be taken into consideration[33].

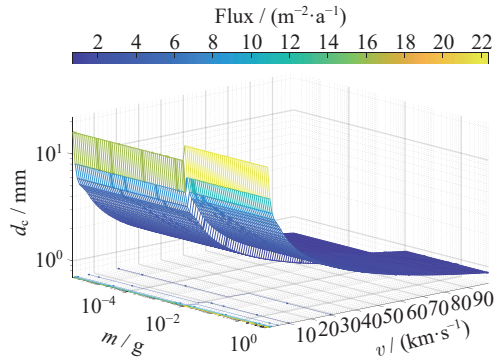

Fig. 13 Critical diameter d_c as a function of the meteoroid mass and impact velocity, where each line represents the critical diameter for a certain mass and velocity

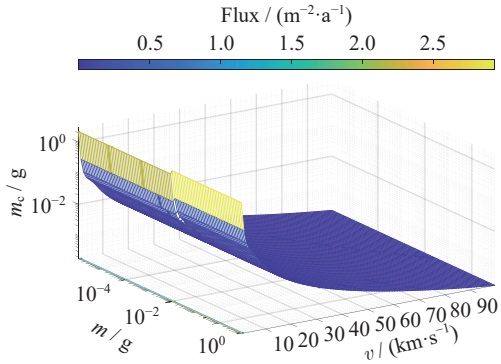

Fig. 14 Critical mass m_c as a function of the meteoroid mass and impact velocity, where each line represents the critical mass for a certain mass and velocity

3 Risk Comparison of the Meteoroid to Space Debris

Currently, it is not necessary to consider the effect of space debris in the Moon orbit space now. This section uses the ORDEM 3.1 model to analyze the space debris environment for the 8 satellites in the Earth orbit space and compare the results to the meteoroid environment.

3.1 Space Debris Flux Analysis

Figure 17 shows the flux of space debris for the 8 satellites orbiting the Earth in terms of the debris size, ranging from 10^{-5} m to 1 m. It can be seen from the figure that the smaller the debris size, the higher the flux. It is obvious that the flux colliding with CSS is significantly

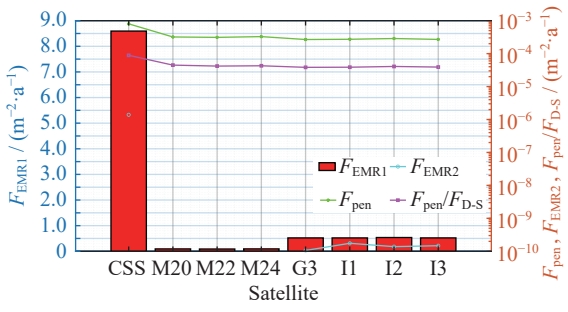

Fig. 15 Catastrophic collision flux F_{EMR1} and F_{EMR2} for 8 satellites orbiting the Earth. The solid green dot indicates the penetrating flux F_{pen} and the magenta square is the ratio of F_{pen} over the total flux $F_{D\text{-}S}$ by the D-S model

higher than that colliding with other satellites. The debris flux for 3 satellites in MEO is higher than that for the 4 satellites in GEO or IGSO. Overall, the debris flux encountering CSS is the highest and the lowest for the satellites in IGSO orbit.

Figure 18 shows the fluxes of space debris with a size greater than 10 μm encountering the satellites with specified impact velocities. Clearly, the debris flux encountering CSS is the highest in any velocity range. Besides, CSS experiences the highest impact velocity of the most space debris.

3.2 Comparison of the Flux of Space Debris to the Meteoroid Flux

The meteoroid investigated in this paper with a mass ranging from 10^{-6} to 10 g is assumed spherical. So is the space debris. From Eq.(3), considering the density of meteoroids and space debris and the output flux results from the ORDEM 3.1 model, we focus on the debris with a diameter larger than 100 μm.

The total fluxes and the impact probabilities for all 11 satellites calculated by each model are shown in Figure 19. These conclusions can be obtained as followed.

(1) Both the flux and probability of CSS encountering space debris with a diameter larger than 100 μm are greater than those of the other 7 satellites in the Earth orbit space, where the flux is about 70.015 $m^{-2}\cdot a^{-1}$ and the impact probability is close to 1, which is mainly due to the debris flux in MEO and GEO is lower than that in LEO. Indeed, the cross-section area of CSS is much larger than 1 m^2, therefore CSS is nearly determined to impact with space debris according to probability statistics. The impact probability of space debris is about 0.86 for the 3 satellites in MEO. The impact probability of

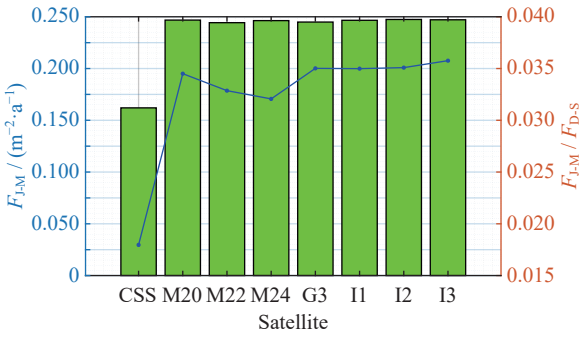

Fig. 16 Total flux $F_{J\text{-}M}$ derived from the J-M model for the 8 satellites (green histogram). The ratio of $F_{J\text{-}M}$ over the total flux $F_{D\text{-}S}$ from the D-S model is demonstrated by the blue asterisk

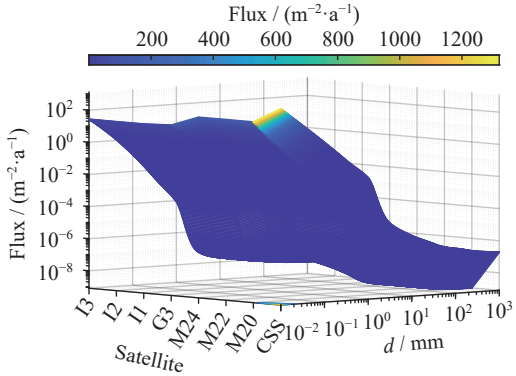

Fig. 17 Space debris flux of the 8 satellites orbiting the Earth in terms of the debris size, where each line represents the flux for a certain satellite and size

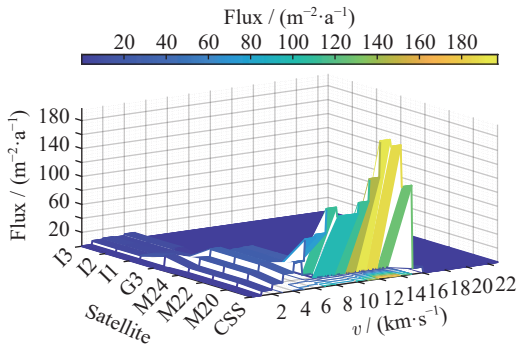

Fig. 18 Fluxes of space debris with a size greater than 10 μm encountering the 8 satellites shown as the function of the impact velocity, where each line represents the flux for a certain satellite and velocity

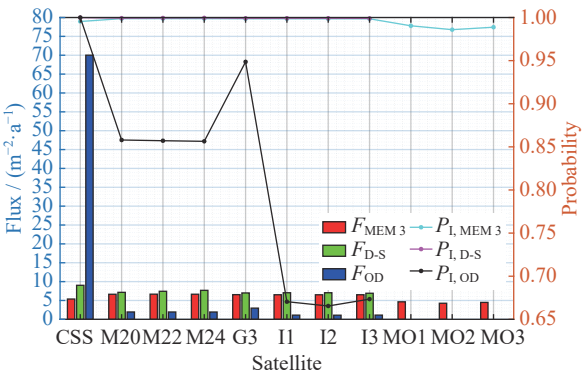

Fig. 19 Model simulated total fluxes and impact probabilities for all satellites

space debris for G3 is about 0.95, slightly higher than that for the MEO satellites, which in some sense reflects the fact that the space activity in GEO is higher than that in IGSO and MEO.

(2) Both the flux and impact probability of satellites encountering the meteoroid in the Earth orbit space are higher than those in the Moon orbit space, which is due to the more significant gravitational focusing effect exerted by the Earth than the Moon.

(3) In the current Earth's space environment, with the exception of CSS, the flux of the other 7 satellites encountering meteoroids is higher than that of space debris of a size larger than 100 μm, consistent with the result that the impact probability of meteoroids is higher than that of space debris, with the former approaching 1.

4 Conclusions

The risk from the hypervelocity impact of meteoroids and orbital debris should be considered for any spacecraft design, hence developers should take protective measures including but not limited to adding extra shielding or placing sensitive equipment at a safer location inside the spacecraft [34]. This paper conducts a systematic and holistic risk assessment of meteoroids and space debris for the BDS-3 satellite constellation first, and compares it with the CSS. In addition, the impact directions of the meteoroids of the 3 satellites orbiting the Moon are also discussed. Several models are used and the results are compared to assess the meteoroid and space debris environment. These conclusions can be drawn as followed.

(1) Model MEM 3 yields a result that the averaged flux of the low-density meteoroid population is lower than that of the high-density population whereas the averaged impact velocity is just the opposite.

(2) The dependence of both averaged flux and impact velocity on the orbital inclination is more pronounced for the surface facing the Earth or the Moon than in the other 8 directions.

(3) For the 8 satellites orbiting the Earth, the catastrophic collision flux of meteoroids computed by the D-S model is greatly reduced after adopting the double-layer Whipple protection measure, and the penetrating flux is less than 1×10^{-3} $m^{-2}\cdot a^{-1}$.

(4) In the Earth's orbit space, the ratio of stream flux over meteoroid flux is less than 0.04. Therefore, in many cases, the impact of the meteoroid stream on spacecraft can be ignored when assessing the meteoroid risk.

(5) According to the above comparison results about the space debris and meteoroid environments with the size larger than 100 μm (corresponding to 10^{-6} g) of these satellites, it can be deduced that the impact risk of space debris should be gained more priority when considering protection for CSS, while for the 7 satellites of BDS-3, the impact risk of meteoroids needs to be paid more attention.

All the spacecraft selected in this paper are in orbit, thus, the results of this paper can act as guidance for the safeguard of operation or for the optimized protection adjustment. In the future, more satellites and spacecraft can be brought into this set of analyses to reveal the relationship between the flux, impact velocity, and impact probability of meteoroids and space debris, and the orientation, orbital altitude, and inclination of these artificial celestial bodies.

References

[1] REN S Y, YANG X H, WANG R L, *et al*. The interaction between the LEO satellite constellation and the space debris environment[J]. *Applied Sciences*, 2021, **11**(20): 9490

[2] ADAMIŠINOVÁ A. European Space Traffic Management System: Micrometeoroids and Space Debris as a Possible Threat for Future Missions[R]. Brno: Mendel University, 2022

[3] BOLEY A C, BYERS M. Satellite mega-constellations create risks in Low Earth Orbit, the atmosphere and on Earth[J]. *Scientific Reports*, 2021, **11**(1): 10642

[4] DUZELLIER S, GORDO P, MELICIO R, *et al*. Space debris generation in GEO: Space materials testing and evaluation[J]. *Acta Astronautica*, 2022, **192**: 258-275

[5] OIKONOMIDOU X, BRAUN V, LEMMENS S. Guidelines for space debris and meteoroid impact risk assessment with DRAMA/MIDAS[C]//8 th European Conference on Space Debris. Darmstadt, Germany: ESA Space Debris Office, 2021

[6] COOKE W, MATNEY M, MOORHEAD A V, *et al*. A comparison of damaging meteoroid and orbital debris fluxes in earth orbit[C]//7 th European Conference on Space Debris. Darmstadt, Germany: ESA Space Debris Office, 2017

[7] MOORHEAD A V, MATNEY M. The ratio of hazardous meteoroids to orbital debris in near-earth space[J]. *Advances in Space Research*, 2021, **67**(1): 384-392

[8] KRAG H, SERRANO M, BRAUN V, *et al*. A 1 cm space

debris impact onto the Sentinel-1 A solar array[J]. *Acta Astronautica*, 2017, **137**: 434-443

[9] HOFFMAN K D, HYDE J L, CHRISTIANSEN E L, *et al*. Extravehicular activity micrometeoroid and orbital debris risk assessment methodology[C]//Proceedings of the 2019 Hypervelocity Impact Symposium. Destin, FL, USA: American Society of Mechanical Engineers, 2019

[10] HOFFMAN K, HYDE J L, CHRISTIANSEN E L, *et al*. Comparison of risk from orbital debris and meteoroid environment models on the Extravehicular Mobility Unit (EMU)[C]//Proceedings of the 1 st International Orbital Debris Conference (IOC). Houston, Texas, United States, 2019

[11] EVANS H J, HYDE J L, CHRISTANSEN E L, *et al*. Consequences of micrometeoroid/orbital debris penetrations on the international space station[C]//Proceedings of the 2019 Hypervelocity Impact Symposium. Destin, FL, USA: American Society of Mechanical Engineers, 2019

[12] HYDE J L, CHRISTIANSEN E L, LEAR D M, *et al*. Surveys of returned ISS hardware for MMMOD impacts[C]//Proceedings of the 7 th European Conference on Space Debris. Darmstadt, Germany: ESA, 2017

[13] OLIVIERI L, FRANCESCONI A. Large constellations assessment and optimization in LEO space debris environment[J]. *Advances in Space Research*, 2020, **65**(1): 351-363

[14] PANOV D V, SILNIKOV M V, MIKHAYLIN A I, *et al*. Large-scale shielding structures in low earth orbits[J]. *Acta Astronautica*, 2015, **109**: 153-161

[15] Moorhead A V. NASA Meteoroid Engineering Model (MEM) Version 3[R]. 2020.

[16] EHLERT S. Modeling meteoroid densities for spacecraft risk assessment[J]. *Journal of Space Safety Engineering*, 2020, **7**(3): 249-254

[17] BRAUN V, HORSTMANN A, LEMMENS S, *et al*. Recent developments in space debris environment modelling, verification and validation with MASTER[C]//Proceedings of the 8 th European Conference on Space Debris. Darmstadt, Germany: ESA Space Debris Office, 2021

[18] BRAUN V. Impact of debris model updates on risk assessments[C]//Proceedings of the 1 st NEO and Space Debris Detection Conference. Darmstadt, Germany: ESA Space Debris Office, 2019

[19] Flegel S, Gelhaus J, Möckel M, *et al*. Maintenance of the ESA MASTER Model[J]. Final Report, 2011, 21705(08)

[20] JENNISKENS P. Meteor stream activity I. The annual streams[J]. *Astronomy and Astrophysics*, 1994, **287**: 990-1013

[21] Vavrin, Andrew B. , *et al*. NASA Orbital Debris Engineering Model ORDEM 3.1-Software User Guide. No. JSC-E-DAA-TN75767. 2019

[22] MANIS A, MATNEY M, ANZ-MEADOR P, *et al*. The Updated GEO Population for ORDEM 3.1[C]//Proceedings of the 1 st International Orbital Debris Conference. Houston, Texas, United States, 2019

[23] RODMANN J, MILLER A, TRAUD M, *et al*. Micrometeoroid impact risk assessment for interplanetary missions//8 th European Conference on Space Debris. Darmstadt, Germany: ESA Space Debris Office, 2021

[24] RYAN S, CHRISTIANSEN E L. A ballistic limit analysis programme for shielding against micrometeoroids and orbital debris[J]. *Acta Astronautica*, 2011, **69**(5/6): 245-257

[25] CHRISTIANSEN E L. Design and performance equations for advanced meteoroid and debris shields[J]. *International Journal of Impact Engineering*, 1993, **14**(1/4): 145-156

[26] MOORHEAD A V, KINGERY A, EHLERT S. NASA's meteoroid engineering model 3 and its ability to replicate spacecraft impact rates[J]. *Journal of Spacecraft and Rockets*, 2020, **57**(1): 160-176

[27] BUSLOV E P, KOMAROV I S, SELIVANOV V V, *et al*. Protection of inflatable modules of orbital stations against impacts of particles of space debris[J]. *Acta Astronautica*, 2019, **163**: 54-61

[28] LE MAY S, GEHLY S, CARTER B A, *et al*. Space debris collision probability analysis for proposed global broadband constellations[J]. *Acta Astronautica*, 2018, **151**: 445-455

[29] TORKY M, HASSANEIN A E, EL FIKY A H, *et al*. Analyzing space debris flux and predicting satellites collision probability in LEO orbits based on petri nets[J]. *IEEE Access*, 2019, **7**: 83461-83473

[30] Christiansen, Eric L. Meteoroid/debris shielding. No. S-898. Houston: National Aeronautics and Space Administration, Lyndon B. Johnson Space Center, 2003

[31] HU D Q, CHI R Q, LIU Y Y, *et al*. Sensitivity analysis of spacecraft in micrometeoroids and orbital debris environment based on panel method[J]. *Defence Technology*, 2023, **19**: 126-142

[32] MOORHEAD A V. Meteoroid environment modeling: The meteoroid engineering model and shower forecasting[C]//Proceedings of the Applied Space Environments Conference (ASEC) 2017: Measurements, Models, Testing & Tools. Huntsville, AL USA, 2017

[33] MURTAZOV A K. Assessing the meteoroid risk in near earth space[J]. *Open Astronomy*, 2018, **27**(1): 144-149

[34] DROLSHAGEN G. Impact effects from small size meteoroids and space debris[J]. *Advances in Space Research*, 2008, **41**(7): 1123-1131